jmb Article

Three-Dimensional Model for the Human Cl^-/HCO_3^- Exchanger, AE1, by Homology to the *E. coli* ClC Protein

Pamela Bonar[1], Hans-Peter Schneider[2], Holger M. Becker[3], Joachim W. Deitmer[2] and Joseph R. Casey[1]

1 - Membrane Protein Disease Research Group, *Department of Biochemistry, University of Alberta, Edmonton, Canada T6G 2H7*
2 - Abteilung für Allgemeine Zoologie, *Fachbereich Biologie, Technische Universtät Kaiserslautern, D-67653 Kaiserslautern, Germany*
3 - Arbeitsgruppe Zoologie/Membrantransport, *Fachbereich Biologie, Technische Universtät Kaiserslautern, P.O. Box 3049, 67653 Kaiserslautern, Germany*

Correspondence to Joseph R. Casey: *joe.casey@ualberta.ca*
http://dx.doi.org/10.1016/j.jmb.2013.04.005
Edited by J. Bowie

Abstract

AE1 mediates electroneutral 1:1 exchange of bicarbonate for chloride across the plasma membrane of erythrocytes and type A cells of the renal collecting duct. No high-resolution structure is available for the AE1 membrane domain, which alone is required for its transport activity. A recent electron microscopy structure of the AE1 membrane domain was proposed to have a similar protein fold to ClC chloride channels. We developed a three-dimensional homology model of the AE1 membrane domain, using the *Escherichia coli* ClC channel structure as a template. This model agrees well with a long list of biochemically established spatial constraints for AE1. To investigate the AE1 transport mechanism, we created point mutations in regions corresponding to *E. coli* ClC transport mechanism residues. When expressed in HEK293 cells, several mutants had Cl^-/HCO_3^- exchange rates significantly different from that of wild-type AE1. When further assessed in *Xenopus laevis* oocytes, there were significant changes in the transport activity of several AE1 point mutants as assessed by changes in pH. None of the mutants, however, added an electrogenic component to AE1 transport activity. This indicates that the AE1 point mutants altered the transport activity of AE1, without changing its electrogenicity and stoichiometry. The homology model successfully identified residues in AE1 that are critical to AE1 transport activity. Thus, we conclude that AE1 has a similar protein fold to ClC chloride channels.

© 2013 The Authors. Published by Elsevier Ltd. Open access under CC BY license.

Introduction

AE1, also known as Band 3 or SLC4A1, is a member of the SLC4 family of bicarbonate transporters.[1] More specifically, AE1 belongs to a sub-family of 1:1 electroneutral chloride/bicarbonate exchangers, which includes AE2 and AE3.[1] In erythrocytes, AE1, which comprises 50% of membrane protein, is essential to maintain the biconcave disc structure and to maximize the HCO_3^- carrying capacity of the blood.[2] In the renal collecting duct, AE1 functions in bicarbonate reabsorption to prevent systemic acidosis.[1] Mutations in AE1 cause blood and renal diseases, including hereditary spherocytosis and distal renal tubular acidosis, respectively.[1]

AE1 is composed of two domains, a 43-kDa N-terminal cytoplasmic domain and a 55-kDa integral membrane domain with 12–14 transmembrane segments.[3] The AE1 cytoplasmic domain forms numerous protein–protein interactions that anchor the erythrocyte cytoskeleton to the plasma membrane,[2] while the membrane domain alone is responsible for AE1 transport activity.[4] Although there is a 2.6-Å-resolution structure of the AE1 cytoplasmic domain,[5] structural information on the membrane domain is far more limited. Many studies have investigated the topology,[3,6–15] oligomerization,[16] helical packing,[17,18] and overall three-dimensional structure of human AE1,[19–23] as a result of its abundance and ease of purification from

erythrocytes.[24] Structural studies of human erythrocyte AE1 membrane domain yielded several low-resolution structures of AE1.[19,21–23] Thus far, the highest resolution structure (7.5–16 Å) was obtained by two-dimensional crystallization and electron microscopy.[19] This resolution does not allow determination of helical packing of the entire membrane domain and the placement of individual amino acids. Still, structural similarity between short regions of AE1 and ClC led to the proposal that AE1 has the same fold as the ClC family of chloride transporters.[19]

The ClC family of chloride transporters comprises nine isoforms in humans that divide into three subfamilies: vesicular $2Cl^-/H^+$ exchangers, plasma membrane Cl^- channels, and ambiguous ClC transporters.[25] Structures of prokaryotic and eukaryotic ClC proteins led to a model for the transport mechanism of ClCs.[26–28] Much of the structural and functional data available are from the *Escherichia coli* ClC protein, which is thus the focus of the current study. Three Cl^- binding sites were identified in ClC structures.[26–28] At the external Cl^- binding site, an extracellular glutamate gate (E148) is required for the transport activity.[26] Protonation of this site is proposed to open or close the gate, allowing movement of Cl^- through the transporter.[27] In the central Cl^- binding site of *E. coli* ClC, the side chains of S107 and Y445 and the main-chain amide groups of I356 and F357 together coordinate the Cl^- ion.[26] An intracellular glutamate gate, E203 of *E. coli* ClC, is involved only in the coupling of H^+ exchange to Cl^- transport.[29] This gate is distant from the intracellular Cl^- translocation pathway, and the mechanism of H^+ transport to this site is not known.

While AE1 and ClC proteins do not have a high sequence similarity, which is often considered a requirement for homology modeling, the proteins share many other similarities. ClC proteins and AE1 both form dimers whose monomers function independently.[16,30,31] *E. coli* ClC performs $2Cl^-/H^+$ exchange at a rate of 2.1×10^3 ions/s,[32] which is much faster than classical membrane transporters; AE1 has a transport rate of 5×10^4 ions/s,[33] and is even faster than *E. coli* ClC, but still slower than an ion channel flux. The proposed ClC transport mechanism is amenable to a fast transport rate, as it only requires subtle movements of residue side chains and not whole helices. ClC and AE1 are also involved in Cl^- transport coupled to the exchange of a H^+ equivalent, H^+ for ClCs and HCO_3^- for AE1. Interestingly, two other bicarbonate transporters, SLC26A3 and SLC26A6, have been modeled on the structure of the *E. coli* ClC.[34] The SLC26 proteins, however, arose from a different evolutionary lineage than SLC4 proteins and thus do not share sequence homology with SLC4 proteins.[1]

On the basis of an AE1 topology model, created using an *E. coli* ClC structure as a template,[35] we constructed a three-dimensional AE1 homology. This model agrees well with existing biochemical constraints, and residues corresponding to ClC transport mechanism residues were in large part similar. When these potential transport mechanism residues were mutated in AE1, there was a significant effect on AE1 transport activity. We propose that AE1 has a similar protein fold and transport mechanism as ClC chloride channels.

Results

Creation of an AE1 model structure

We set out to develop a three-dimensional homology model of the human AE1 membrane domain. The GenTHREADER program† predicts that the *E. coli* ClC structure is a candidate for AE1 homology modeling (Supplementary Table 1). Other candidate proteins were either from the importin/exportin family of nuclear transport proteins or from integral transmembrane transport proteins (Supplementary Table 1). The importin/exportin protein family was excluded since they are soluble proteins, which bind to macromolecules (such as RNA) and are transported through the nuclear pore complex. The remaining candidate structures were used to create crude sequence alignments and homology models. Even with manual adjustments, the AE1 homology models created, using these structures as templates, did not satisfy basic biochemical constraints for AE1 (not shown). All of these models had incorrect orientations of the N-terminus, C-terminus, or glycosylation site relative to the lipid bilayer. In the list of candidates generated by GenTHREADER, only *E. coli* ClC acted as a template producing a satisfactory model. This provides the first evidence that ClC proteins provide a suitable structural model for AE1.

Further evidence for structural similarities between AE1 and ClC were provided by a recent 7.5- to 16-Å structure of AE1 suggesting that AE1 has the same fold as ClC chloride channels.[19] A subsequent paper elaborated on an alignment between AE1 and *E. coli* ClC.[35] Here, this alignment was modified to create a sequence alignment between *E. coli* ClC residues and the human AE1 membrane domain (amino acids 388–911, Fig. 1). Sequence alignment gaps between AE1 E480–S525 and T728–G838, corresponding to ClC V122–D171 and G316–A404, respectively, were minimized to increase the amount of sequence similarity. In addition, minimization of sequence alignment gaps in AE1 E480–S525 allowed for AE1 E508 to directly correspond with the ClC extracellular glutamate gate (Fig. 1). Alterations to sequence alignment gaps in AE1 T728–G838 also increased the agreement between the

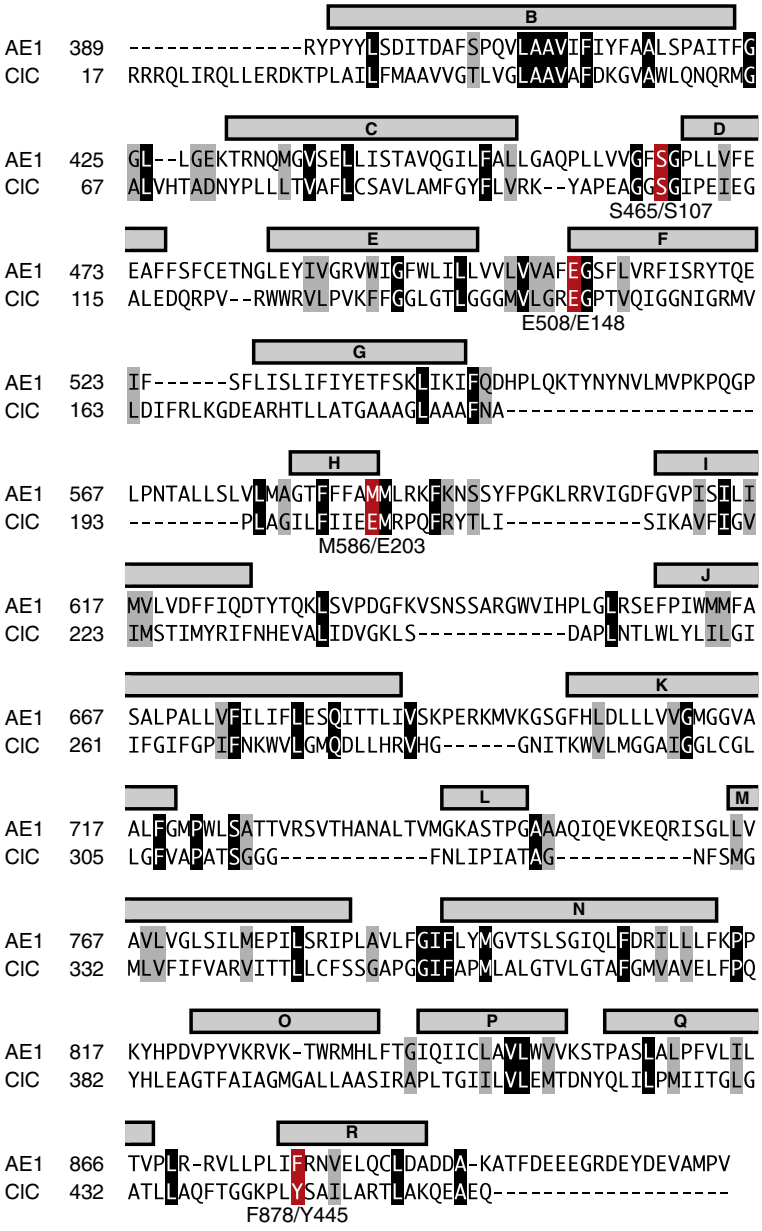

Fig. 1. AE1 and ClC amino acid sequence alignment. The sequences of the human AE1 membrane domain (amino acids 388–911) and *E. coli* ClC were aligned on the basis of a published structural alignment,[35] with minor manual adjustments. Identical residues in the sequence alignment are black and similar residues are gray. Residues involved in the ClC transport mechanism and the corresponding AE1 residues are red, with the corresponding residue numbers indicated beneath (AE1/ClC). Transmembrane-spanning segments, following the assignment in the original ClC crystal structure,[26] are indicated and labeled from B to R.

AE1 homology model and data from AE1 cysteine-scanning mutagenesis studies.[3,7] This alignment method was used instead of traditional sequence alignment algorithms, since the sequence similarity between human AE1 and *E. coli* ClC is too low (9.8% identical and 18.4% similar). As a result, traditional sequence alignments had large gaps in transmembrane-spanning helices, and the models generated using these sequence alignments did not satisfy basic AE1 biochemical constraints.

The amino acid sequence alignment (Fig. 1) was used to generate a homology model of AE1, on the basis of the *E. coli* ClC structure.[26] The AE1 homology model, created using the program Modeller v9.7,[36] is shown with the template *E. coli* ClC structure overlaid (Fig. 2). The root-mean-square deviation between the AE1 homology model and the template ClC structure is 0.8 Å, as determined by the pairwise structural alignment function on the Dali server‡.

Evaluation of the AE1 homology model by comparison to substituted cysteine accessibility data and blood group antigens

AE1 cysteine-scanning mutagenesis studies measured residue accessibility to biotin maleimide (Supplementary Table 2).[3,6,7,17] To assess the agreement of the AE1 homology model with these biochemical spatial constraints, we plotted the

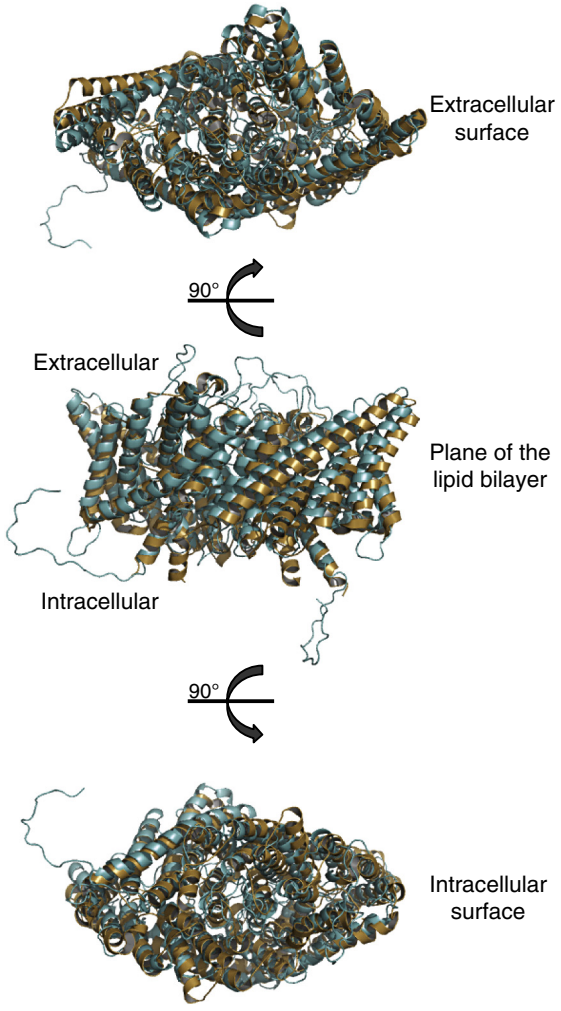

Fig. 2. Homology model of the AE1 membrane domain, using the *E. coli* ClC structure. A homology model of the human AE1 integral membrane domain (residues 388–911) was created using Modeller v9.7. The AE1 homology model is shown as a dimer in teal and the template ClC structure is shown in beige. Three views of the structure are shown, looking parallel to the lipid bilayer, to the extracellular side, and to the intracellular side.

biotinylation levels of cysteine mutants on the AE1 homology model (Fig. 3). The degree of biotinylation by biotin maleimide correlates with aqueous accessibility of the residue. All AE1 cysteine-scanning mutagenic studies were normalized to the amount of Y555C-AE1 biotinylation, a site that is highly aqueous accessible.[3,6,7,17] In the AE1 homology model, the majority of cysteine mutants with $<10\%$ biotinylation are located within the plane of the lipid bilayer as expected. In contrast, the majority of cysteine mutants with $>50\%$ biotinylation are located in extracellular or intracellular accessible regions of the AE1 homology model. Cysteine mutants with low levels of biotinylation (10–30%) or moderate levels of biotinylation (30–50%) clustered in regions near the interface between the plane of the lipid bilayer and extra/intracellular surfaces of the AE1 homology model.

In addition, all eight blood group antigens attributed to an AE1 sequence (Supplementary Table 2) and the N-linked glycosylation site (N642) were appropriately located on the extracellular surface of the AE1 homology model (Fig. 3b).[10,15,37] Thus, the AE1 homology model is fundamentally consistent with previously published biochemical data gathered from cysteine-scanning mutagenesis and blood group antigen mapping.

Identification of residues possibly involved in the AE1 transport mechanism

Interestingly, although the amino acid sequence alignment shows low sequence similarity, all of the residues involved in the ClC transport mechanism are identical with or similar to the corresponding residues in the AE1 homology model (Fig. 4). The sole exception is the intracellular glutamate gate (E203) in ClC, located 13 Å away from the central Cl^- binding site, which corresponds to M586 in AE1 (Fig. 4). Since this residue is not similar to the intracellular glutamate gate of ClC, we considered two other candidate residues that could fulfill this role. The closest acidic residue in the AE1 primary sequence is D607, which is located 27 Å away from the central Cl^- binding site in the homology model (Fig. 4c). In addition, AE1 E681 has a key role in AE1 transport activity[38–40] and is 14 Å away from the central Cl^- binding site (Fig. 4c). The extracellular glutamate gate of ClC is E148, and the corresponding residue in the AE1 homology model is E508. S107 and Y445 form the central Cl^--binding site of ClC through their side-chain moieties, and the corresponding residues in the AE1 homology model are S465 and F878 (Fig. 4).

Transport activity of AE1 point mutants assessed in HEK293 cells

To test the validity of the AE1 homology model, we mutated all of the identified candidate AE1 transport mechanism residues to alanine. As well, D607 was mutated, since it is an AE1 intracellular glutamate gate candidate. We chose not to investigate AE1 E681, although it is also an AE1 intracellular glutamate gate candidate, since the role of E681 in AE1 transport activity is established.[38,40] To examine whether the effects on AE1 transport activity were directly attributed to a functional role of the single point mutation, or if the point mutation was located in a region sensitive to mutagenesis, we also mutated the four residues flanking each candidate transport mechanism site (Fig. 4).

Transport activity of AE1 mutants was assessed by Cl^-/HCO_3^- exchange activity assays (Fig. 5).

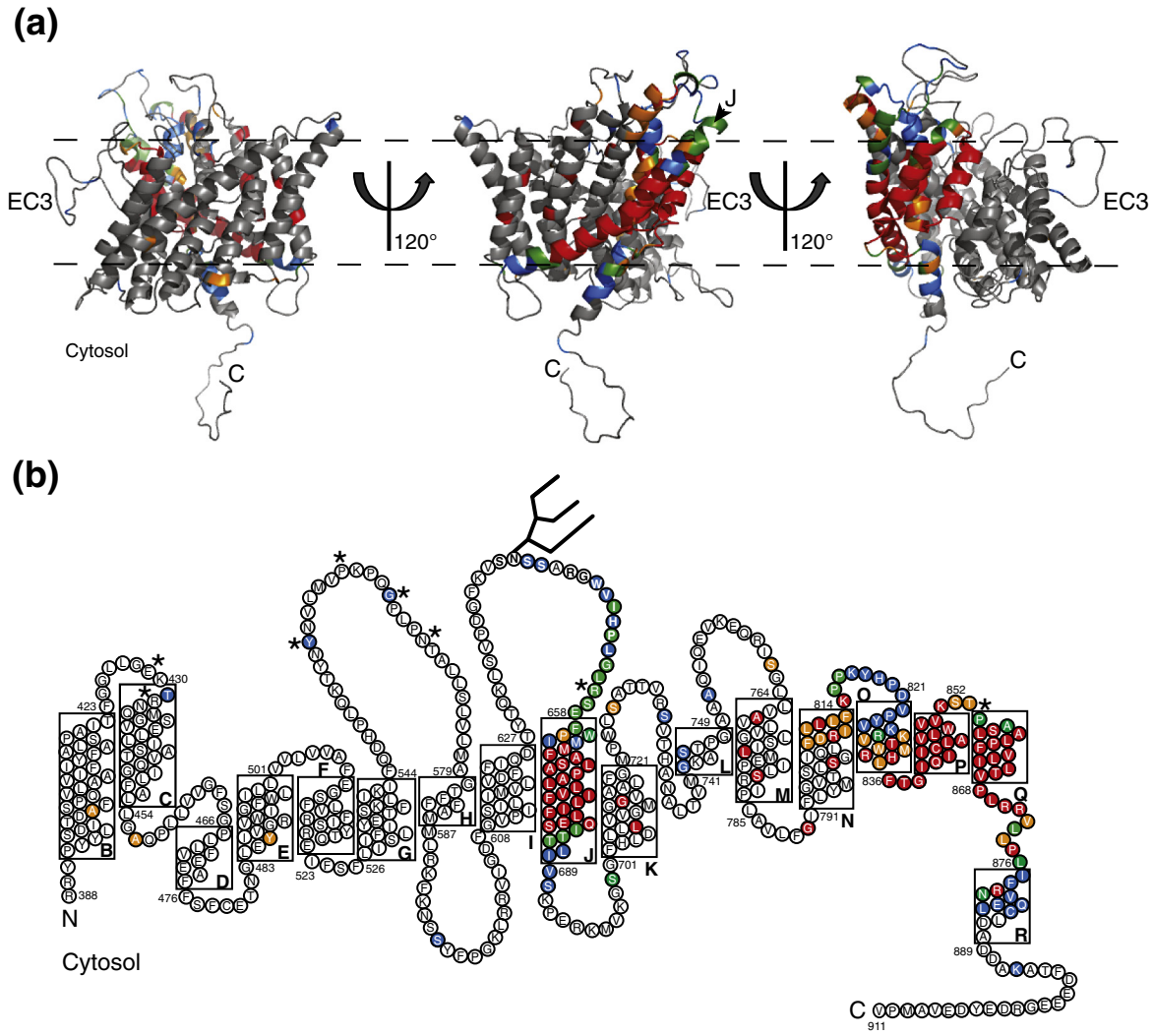

Fig. 3. Evaluation of the AE1 homology model, using existing biochemical constraints. AE1 spatial constraints from published cysteine-scanning mutagenesis studies were used to examine the validity of the AE1 homology model. Mutagenized amino acids in AE1 were colored according to the level of biotin maleimide incorporation (corresponding to aqueous accessibility).[3,6,7,17] Cysteine mutants with <10% biotinylation are in red, those with 10–30% biotinylation are in orange, those with 30–50% biotinylation are in green, and those with >50% biotinylation are in blue. Gray (a) or white (b) indicates no data available. (a) An AE1 homology model monomer, with three different orientations parallel to the lipid bilayer. C marks the cytosolic C-terminus of AE1, broken lines represent the approximate boundaries of the lipid bilayer, and EC3 marks AE1 extracellular loop 3. In the middle panel, the N-terminus of transmembrane helix J is indicated with an arrowhead. The dimer interface of the AE1 homology model faces the reader in the right panel. (b) Topology model of AE1, based on the three-dimensional homology model. Transmembrane-spanning segments are indicated and labeled from B to R. The N-linked glycosylation site is indicated by a large branched structure and sites of blood group antigens (Supplementary Table 2) are indicated by an asterisk (*). The N-terminus and C-terminus are indicated by N and C, respectively.

HEK293 cells grown on glass coverslips were transiently transfected with cDNA encoding wild-type (WT)-AE1, an AE1 point mutant, or vector. Cells were subsequently loaded with the pH-sensitive dye, BCECF-AM [2′,7′-bis-(2-carboxyethyl)-5-(and-6)carboxylfluorescein, acetoxymethyl ester], and cells were alternately perfused with CO_2-bubbled Cl^--containing and Cl^--free Ringer's buffer. In AE1-transfected cells, switching from a Cl^--containing to a Cl^--free Ringer's buffer induced cytosolic alkalinization due to AE1-mediated Cl^- efflux and HCO_3^- influx (Fig. 5a). In comparison, vector-transfected cells had a low background rate of alkalinization, following the switch from Cl^--containing to Cl^--free Ringer's buffer (Fig. 5b). Bicarbonate transport rates were calculated by linear regression of the initial rate of cytosolic alkalinization upon switching to Cl^--free Ringer's buffer. Bicarbonate transport rates were

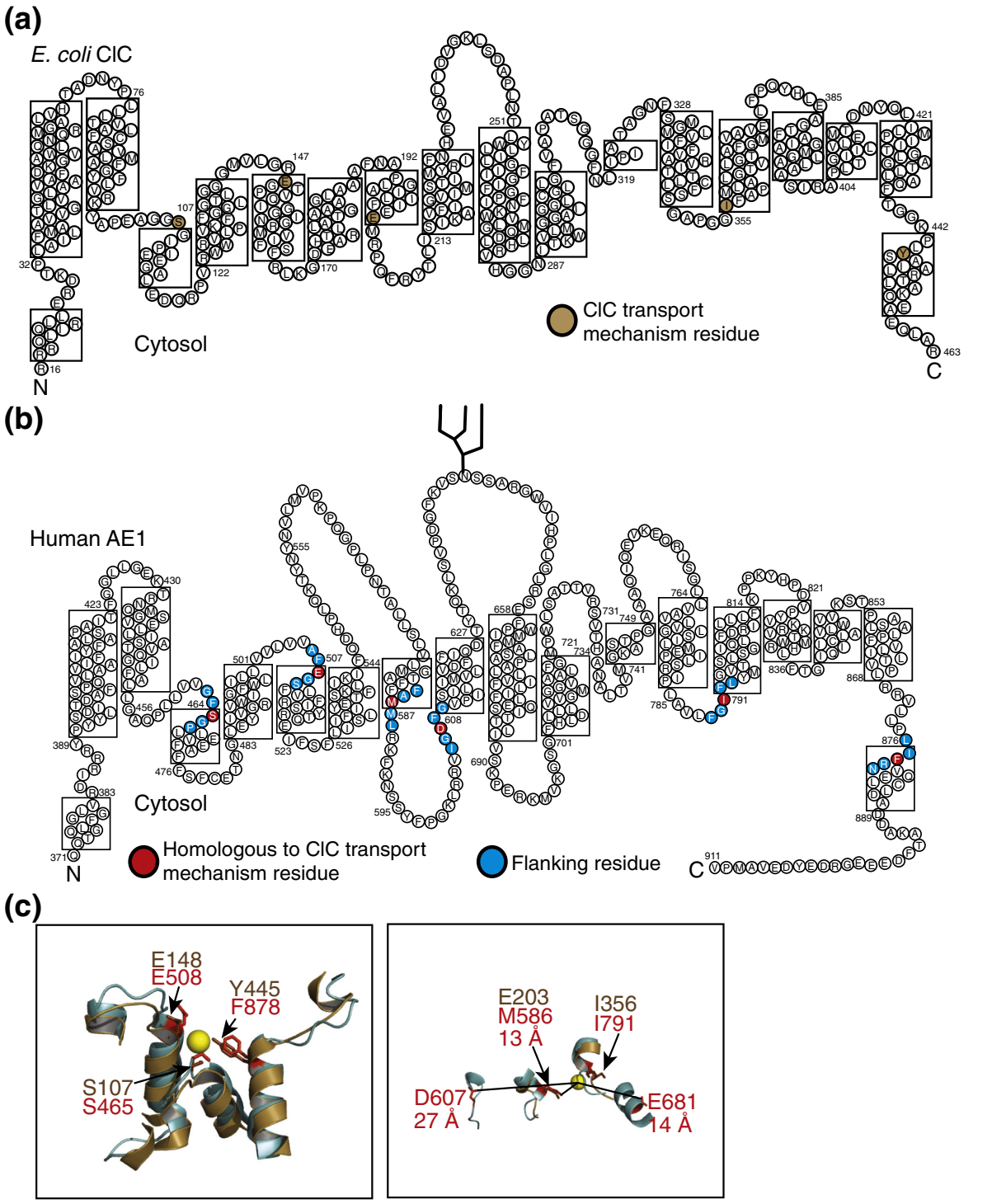

Fig. 4. Identification of possible transport mechanism residues. (a) In the *E. coli* ClC topology model, residues involved in the transport mechanism of ClC are colored beige. (b) In the AE1 topology model, candidate transport mechanism residues are colored red and flanking residues are colored blue. The N-terminus and C-terminus are indicated by N and C, respectively. (c) Three-dimensional structure of the central Cl^- coordination site, with two different views (left and right panels). The ClC structure is shown in beige and the residues involved in the transport mechanism are indicated in brown. The AE1 homology model is shown with residues corresponding to residues in ClC involved in the transport mechanism indicated in red and flanking residues indicated in teal. A yellow sphere represents a Cl^- in the central Cl^- coordination site. In the right panel, distances between AE1 residues and Cl^- are marked by black lines and indicated in red below the corresponding AE1 residue.

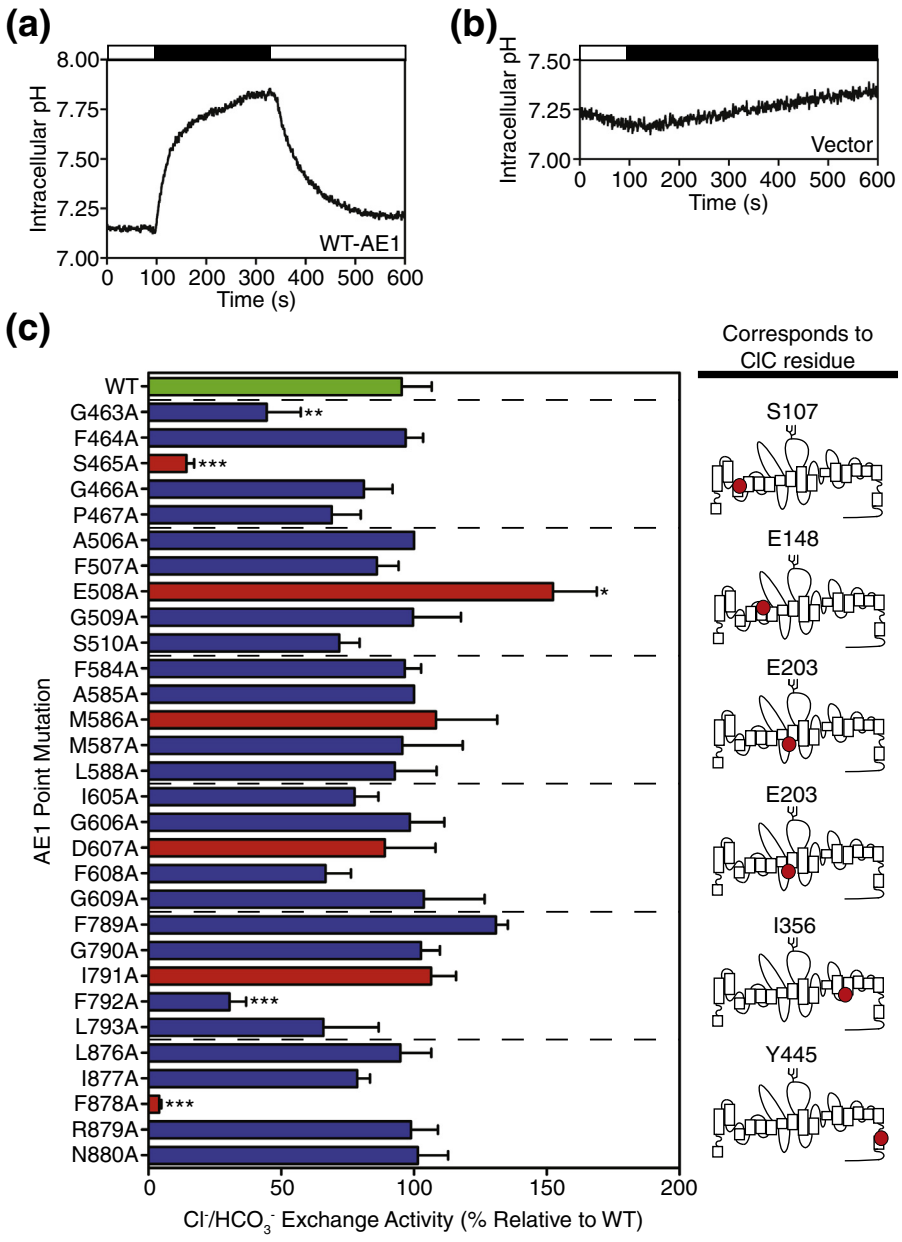

Fig. 5. Transport activity of AE1 alanine point mutants. HEK293 cells were grown on glass coverslips and transiently transfected with cDNA encoding WT-type AE1 (a), an AE1 alanine point mutant, or vector (b). Cells were loaded with the pH-sensitive dye, BCECF-AM, and fluorescence was monitored as cells were alternately perfused with Ringer's buffer containing sodium chloride (open bar), or chloride-free Ringer's buffer (black bar). Transport rates were monitored by the rate of alkalinization induced upon switching to chloride-free medium. (c) Anion-exchange activity was measured for WT-AE1 and alanine point mutants, with the corresponding ClC transport mechanism residues indicated in the topology models. The bar graph shows transport rates corrected for background and normalized to protein expression and cell surface processing. Anion-exchange activity was measured and plotted relative to WT. Error bars represent SE (n = 3–6), and asterisk (*) indicates a significance difference from WT ($p < 0.05$).

subsequently corrected for background in vector-transfected HEK293 cells and normalized for the amount of protein expressed at the cell surface (Supplementary Figs. 1 and 2).

The Cl^- coordinating residue, S107, of ClC corresponds to AE1 S465. Thus, we investigated G463A, F464A, S465A, G466A, and P467A-AE1 (Fig. 5c). S465A had a significantly reduced Cl^-/HCO_3^- exchange activity (14 ± 3% compared to WT-AE1). In comparison, flanking mutants F464A, G466A, and P467A had transport activities not significantly different from WT-AE1. G463A had a

transport activity of 44 ± 13%, which was significantly different from WT-AE1. S465N and S465D had significantly reduced transport activity, 6 ± 6% and 5 ± 5%, relative to WT-AE1, respectively (Fig. 6). Transport activity of S465T (43 ± 5% relative to WT-AE1), however, was significantly faster than S465-AE1 transport activity (Fig. 6).

The ClC extracellular glutamate gate (E148) corresponds to E508 in the AE1 homology model. None of the flanking mutants had transport rates significantly different from WT-AE1 (Fig. 5c). In contrast, E508A has a significantly increased transport rate (152 ± 16% compared to WT-AE1), which is remarkable as the transport rate of WT-AE1 is unusually fast for a transporter (5×10^4 ions/s) so it is exceptional to create an AE1 mutant with a higher transport rate than WT-AE1. Similar to E508A-AE1, E508D, E508S, and E508K-AE1 had significantly faster transport activities (186 ± 35%, 210 ± 26%, and 211 ± 55%, respectively) compared to WT-AE1 (Fig. 6). Interestingly, E508Q-AE1 had a transport activity of 75 ± 5%, which was not significantly different from that of WT-AE1 (Fig. 6).

The AE1 residue corresponding to the intracellular glutamate gate of ClC (E203) is M586. Alanine mutants at AE1 M586, D607, and flanking these sites had transport activities not significantly different from that of WT-AE1 (Fig. 5c), which suggests that M586 and D607 are not the functional equivalent of the ClC intracellular glutamate gate, E203.

We investigated the functional role of AE1 I791 and F792, since these residues correspond to ClC I356 and F357, which are involved in Cl^- coordination through their backbone amides. F789A, G790A, I791A, and L793A-AE1 all had transport rates not significantly different from that of WT-AE1 (Fig. 5c). F792A-AE1 had a significantly reduced transport activity (31 ± 6%, compared to WT-AE1). This indicates either that the side chain of F792 is involved in AE1 transport activity or that mutation of F792 causes structural changes in AE1 that alter the transport activity. Since I791A-AE1 is a conservative mutation, we assessed I791S-AE1, which was not significantly different from WT-AE1 (Fig. 6). This confirms that the side chain of I791 is not involved in the AE1 transport mechanism.

ClC Y445 coordinates Cl^- through interactions with the tyrosine hydroxyl. The corresponding residue in AE1 is F878. Mutants flanking AE1 F878 had no significant difference in transport activity relative to WT-AE1 (Fig. 5c). F878A-AE1 had a significantly reduced transport activity (4 ± 1%)

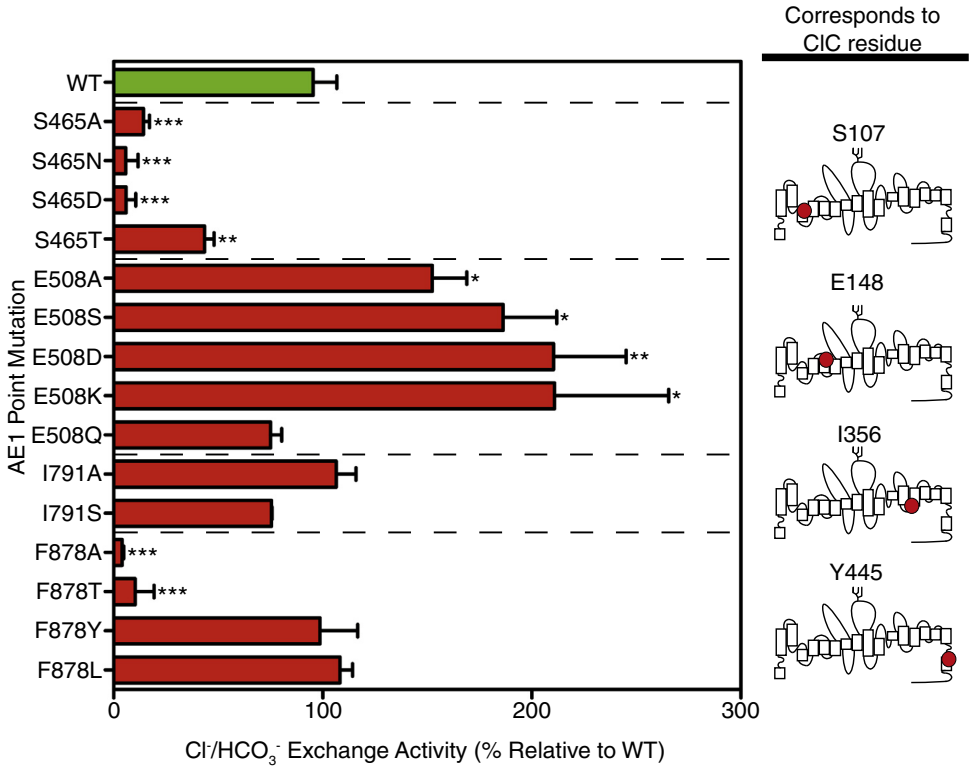

Fig. 6. Functional characterization of AE1 point mutations. Chloride bicarbonate exchange activity of WT and AE1 point mutants was measured in transfected HEK293 cells. Topology models indicate the corresponding ClC transport mechanism residues. The bar graph shows transport rates corrected for background, protein expression, and cell surface processing. Error bars represent SE (n = 3–6), and asterisk (*) indicates a significant difference relative to WT ($p < 0.05$).

compared to WT-AE1 (Fig. 5c). A major reduction in transport activity of F878T-AE1 (10 ± 9% relative to WT-AE1) was also observed (Fig. 6). In contrast, the more conservative F878Y and F878L-AE1 mutants had transport activities not significantly different from WT-AE1 (Fig. 6). Thus, it appears that mutation of AE1 F878 to large hydrophobic or aromatic amino acids has no effect on transport activity, but mutation of AE1 F878 to small hydrophobic or small polar amino acids abolishes transport activity almost completely.

In summary, AE1 residues corresponding to the ClC transport mechanism residues had significant changes in transport activity when mutated. The only exception was AE1 M586, corresponding to the ClC intracellular glutamate gate (E203). In the ClC transport mechanism, this residue is only involved in transport of H^+ coupled to Cl^- transport and is located distant from the central Cl^- coordination site. We hypothesize that E681 of AE1 may fulfill a similar role to the E203 residue of ClC, as this residue in the AE1 homology model is also located on the intracellular side of the lipid bilayer approximately 14 Å away from the central Cl^- binding site and affects AE1 transport activity.[38,40,41]

Transport activity of AE1 point mutants in *Xenopus laevis* oocytes

X. laevis oocytes were co-injected with cRNA encoding WT or mutant AE1 and glycophorin A, or remained non-injected (native) as a control to investigate candidate transport mechanism residues further. Previous studies revealed that optimal cell surface expression of AE1 in oocytes was achieved only when glycophorin A was co-expressed.[42] Cytosolic pH and membrane potential were monitored, using double-barreled microelectrodes inserted just beneath the intracellular surface of the oocyte (Fig. 7). Upon switching from HCO_3^--free oocyte Ringer's solution to high Cl^- oocyte Ringer's solution, a larger acidification was observed in native oocytes than in those expressing WT-AE1 (Fig. 7a and b). This acidification arose from diffusion of the acid, CO_2, into the oocyte. In AE1-expressing oocytes, acidification was minimized by AE1-mediated exchange of extracellular HCO_3^- for intracellular Cl^-.

Similar transport activity data were observed in *X. laevis* oocytes as in HEK293 cells. In *X. laevis* oocytes, M586A, D607A, and I791A-AE1 had transport rates similar to WT-AE1 (Fig. 7d), consistent with results obtained in HEK293 cells. These residues correspond to the intracellular glutamate gate (E203) and the residue (I356) that coordinates Cl^- through its backbone amide in ClC. E508A, S465A, and F878A-AE1, which correspond to the extracellular glutamate gate and Cl^- coordinating residues, all had transport rates significantly different from that of WT-AE1 (34 ± 5%, 56 ± 16%, and 23 ± 5%, respectively, Fig. 7c). While S465A and F878A-AE1 had reduced transport activity when expressed in both HEK293 cells and *X. laevis* oocytes, the reduction in transport activity was smaller in *X. laevis* oocytes than in HEK293 cells. Interestingly, the behavior of E508A-AE1 differs in the two expression systems. In HEK293 cells, E508A has a significantly faster transport rate compared to WT-AE1 but has a significantly slower transport rate in *X. laevis* oocytes.

Application of CO_2/HCO_3^- and reduction of extracellular Cl^- concentration, respectively, did not induce appreciable membrane currents in oocytes expressing WT or mutant AE1. AE1-mediated membrane current (calculated by subtraction of the current measured in native oocytes from the current measured in AE1-expressing oocytes), induced upon switching from high to low Cl^- oocyte Ringer's solution, revealed no significant changes in membrane current between WT-AE1 and AE1 mutants (Fig. 7d). Furthermore, no significant differences in oocyte membrane conductance were observed in WT-AE1 compared to AE1 mutants (Supplementary Fig. 3b). For all transporters expressed, G_m was around 2 μS and was not significantly different from the G_m determined in native oocytes. As for the conductance, no changes in the reversal potential could be detected by expression of WT-AE1 or AE1 mutant (Supplementary Fig. 3c). Thus, none of the AE1 mutations resulted in a shift of transport stoichiometry, which would create an electrogenic AE1 transporter.

Discussion

We developed a three-dimensional AE1 membrane domain homology model, on the basis of the *E. coli* ClC X-ray crystal structure.[26] Leading us to develop this model was the recalcitrance of AE1 to be crystallized because of protein micro-heterogeneity arising from proteolysis and post-translational modifications.[20] The most recent low-resolution structure of the AE1 membrane domain led to the proposal that the AE1 membrane domain shares the protein fold as ClC chloride channels.[19,35] We tested the validity of the AE1 homology model by comparison to published biochemical data, measurements of transport activity, and electrical activity of AE1 mutants assessed in HEK293 cells and *X. laevis* oocytes. Together, the data suggest that AE1 has a fold similar to that of ClC proteins, as well as a similar transport mechanism.

Structural features of the AE1 homology model

The AE1 homology model agrees well with cysteine-scanning mutagenesis data and blood

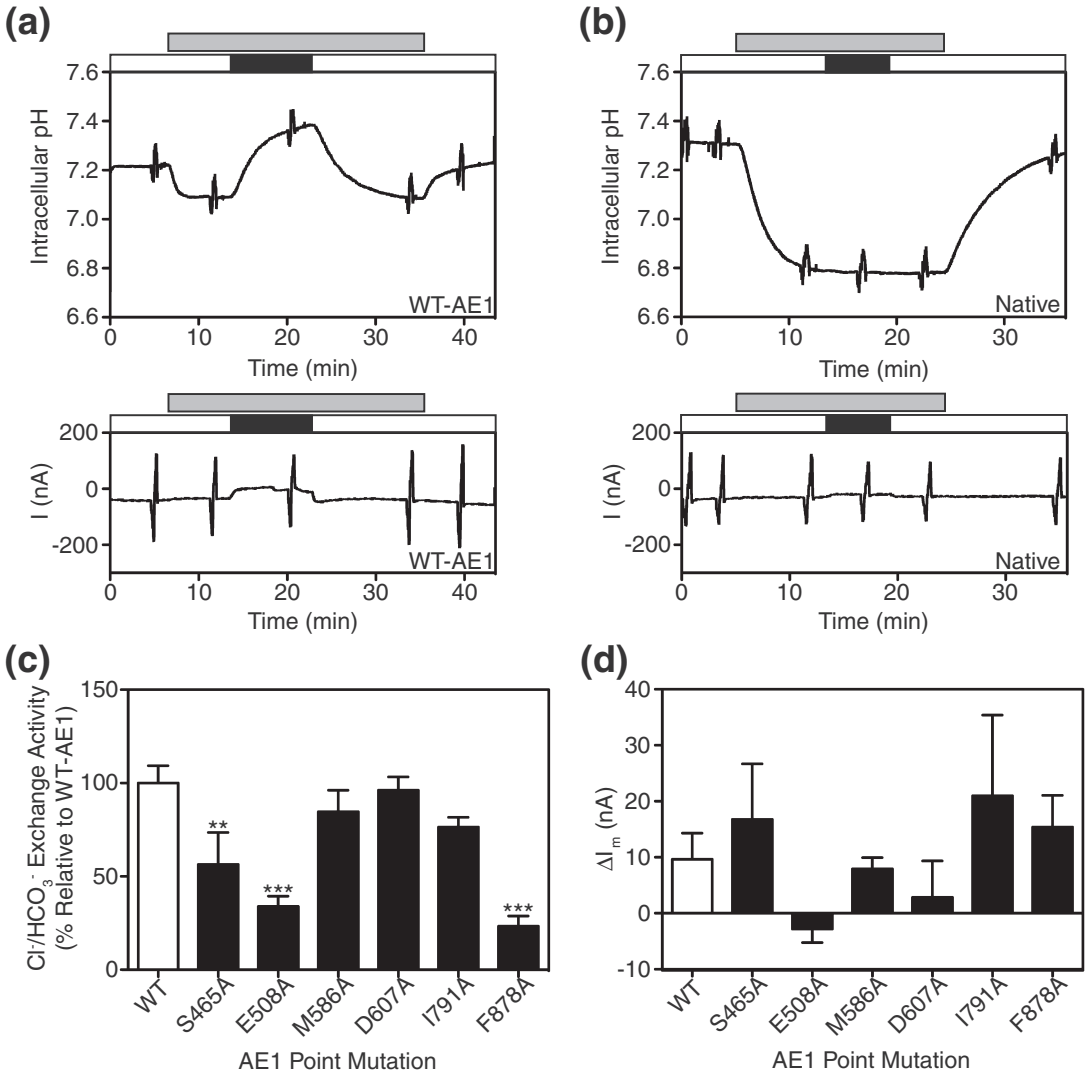

Fig. 7. Characterization of AE1 point mutants in *X. laevis* oocytes. (a) Oocytes were co-injected with cRNA encoding WT-AE1 or a point mutant of AE1 and glycophorin A. (b) Non-injected oocytes were used as a control (native). Current and pH were simultaneously measured using a double-barreled microelectrode combined with two-electrode voltage clamp. Oocytes were perfused with high Cl^- (white bar) and low Cl^- (black bar) solution. The application of CO_2/HCO_3^- is indicated (gray bar). (c) The transport rate was monitored by the rate of alkalinization upon switching from high Cl^- to low Cl^- oocyte Ringer's solution. The bar graph shows transport rates corrected for background activity in native oocytes and plotted relative to WT. (d) AE1-mediated membrane current, induced by switching from high Cl^- to low Cl^- oocyte Ringer's solution, is shown for oocytes expressing WT-AE1 and AE1 mutants. All values were corrected for the difference in current observed in native oocytes. Error bars represent SE (n = 5–13) and asterisk (*) indicates a significant difference from WT ($p < 0.05$).

group antigen data.[3,6,7,10,15,17] Greater discrepancies arise in comparing biochemical evidence for structure of lactose permease and the corresponding crystal structure.[43] The "fit" of AE1 biochemical data may reflect the relatively small conformational changes expected in a high turnover transporter such as AE1. Large conformational changes, evident in the inward and outward states of major facilitator superfamily proteins such as lactose permease,[44] would give rise to biochemical data reflecting a range of conformational states.

In the AE1 homology model, the large third extracellular loop (between transmembrane helices G and H) extends into the lipid bilayer (Fig. 3). When creating the AE1 sequence alignment during homology modeling (Fig. 1), a large gap in the corresponding ClC third extracellular loop was added to accommodate the large AE1 third extracellular loop. Thus, the modeling program (Modeller) could not confidently assign a structure to this region of AE1. While the model shows the region in the bilayer plane, the location of this loop is likely to extend into the extracellular space.

Previous cysteine-scanning mutagenesis predicted M663-S690 to be an unusually long helix extending past the intracellular surface of the lipid bilayer.[6,41] Consistent with this, the corresponding region in the homology model is transmembrane helix J, which spans the lipid bilayer at an angle, making it longer than average transmembrane helices (Fig. 3a).

Proteolytic cleavage data also provide insight into the AE1 homology model (Supplementary Table 2). Several reported AE1 proteolytic cleavage sites[8,9] are located in aqueous accessible extra-/intracellular regions in the AE1 homology model (Fig. 3). The remaining sites (R514, F537, L540, and W831)[8,9] are located in the homology model transmembrane helices (Fig. 3). Much of the proteolytic cleavage data were obtained upon alkaline treatment of AE1, which denatures AE1, making certain cleavage sites more accessible.[8,9] It is likely that the proteolytic cleavage sites within the homology model transmembrane helices are only accessible upon alkaline treatment of AE1, but the studies do not state which cleavage sites are affected by alkaline treatment.[8,9] We do note that chymotryptic cleavage site AE1 W831 (located in transmembrane helix O) is predicted to be in the plane of the lipid bilayer on the basis of lack of biotinylation when mutated to cysteine,[3] strongly suggesting that the proteolysis data are somewhat unreliable in predicting topology.

Additional biochemical data provide insights into the validity of the AE1 model (Supplementary Table 2). Fluorescein maleimide labels AE1 K430 from the extracellular surface,[11] consistent with the AE1 homology model, where AE1 K430 is in the first extracellular loop. AE1 histidine residues (H547, H734, and H834), accessible to the small hydrophilic probe diethylpyrocarbonate,[13] localize to extracellular loops (H547 and H734) or pore lining (H834) in the homology model. Mutagenesis to introduce N-glycosylation acceptor sites at AE1 G428, S633, G637–W648, Q754, and P854 resulted in glycosylation,[14] indicating extracellular localization. In the AE1 homology model, these residues are all located in extracellular loops, consistent with the data. The AE1 inhibitor, H_2DIDS, cross-links residues K539 and K851.[8,45] In the AE1 homology model, both residues are located close to the extracellular surface and the distance between these residues overlaps with the central Cl^- binding site. H_2DIDS is 20 Å long, and in our AE1 model, residues K539–K851 are 22 Å apart. Thus, our model is in good agreement with the ability of H_2DIDS to act as an AE1 inhibitor and cross-link K539–K851 of AE1. The AE1 homology model also has a large cytoplasmic C-terminal domain, and the carbonic anhydrase II binding site (L886–D890) is aqueous accessible (Fig. 3).[46] Taken together, we conclude that the AE1 homology model agrees substantially with biochemical data.

Interestingly, the dimer interface of the AE1 homology model, transmembrane helices H, I, P, and Q (Fig. 3), has structural features consistent with the dimer interface of *E. coli* ClC. The dimer interface of ClC is formed by the hydrophobic interactions of small alkyl residues found in transmembrane helices H, I, P, and Q.[30] Mutation of ClC small alkyl residues in the dimer interface (I201, L406, I422, and L434) to bulky tryptophan residues converted ClC to monomers.[30] While the corresponding residues in the AE1 homology model (F584, Q840, S856, and P868) are not small alkyl residues, there are several flanking small alkyl residues in the corresponding helices, which may form a hydrophobic AE1 dimer interface.

E. coli ClC and AE1 transport mechanisms

In the AE1 homology model, E508 corresponds to the extracellular glutamate gate of ClC (E148). E508A-AE1 had an increased transport activity compared to WT-AE1 when expressed in HEK293 cells. In contrast, E508A-AE1 had a significantly reduced transport activity when expressed in *X. laevis* oocytes. Differences in the two expression systems, such as changes in plasma membrane lipid composition, membrane protein trafficking, and experimental setup, may account for the difference in E508A-AE1 transport activity. Four mutations at AE1 E508 increased AE1 transport activity. Interestingly, only E508Q had activity similar to that of WT-AE1, likely due to similarity in size of glutamine and glutamic acid moieties. Thus, the acidic nature of the glutamic acid side chain is not required to maintain normal AE1 transport activity, but the site is very sensitive to changes in the size and shape of the side chain. In contrast, E148Q-ClC, which removes the glutamate carboxylate group, has H^+ uncoupled Cl^- transport.[47] In both AE1 and ClC, mutation of the residue corresponding to the extracellular glutamate results in significant changes in transport activity; however, the type of changes in transport activity observed and mutations that elicit these changes differ between AE1 and ClC. Interestingly, changes in transport activity of the mutants were not associated with changes in AE1 stoichiometry, which would make the mutants electrogenic transporters (Fig. 7).

In the AE1 homology model, M586 corresponds to the ClC intracellular glutamate gate. This Met residue is not conserved among chicken AE1, human AE2, or human AE3 (Supplementary Fig. 4). Mutation of M586 and the flanking AE1 residues had no effect on the transport activity, nor did mutation of the closest acidic residue in the AE1 amino acid sequence (D607). While the intracellular glutamate gate in ClC is located approximately 15 Å from the central Cl^- binding site, the distance of D607 from this site in the AE1 homology model is almost double (27 Å). For these reasons, D607 of

AE1 is unlikely to be involved in the transport mechanism of AE1.

This led us to AE1 E681 as the most likely candidate to fulfill the role of the intracellular glutamate gate. E681 is located 14 Å away from the central Cl^- binding site in the AE1 homology model, which is similar to the distance between the central Cl^- binding site and intracellular glutamate gate of ClC. Modification or mutation of AE1 E681 alters transport activity by inhibiting monovalent anion exchange, increasing divalent anion transport, and eliminating H^+ co-transport during Cl^-/SO_4^{2-} exchange.[38,40,41] Mutational studies of E203 in ClC (the intracellular glutamate gate) demonstrated that an ionizable side chain is essential for H^+-coupled Cl^- transport by ClC but is not required for independent Cl^- transport.[48] Interestingly, the intracellular glutamate gate of the ClC family is only conserved among $2Cl^-/H^+$ exchanger-type ClC proteins and is a valine residue in channel-like ClC proteins. Thus, another possibility is that Cl^-/HCO_3^- exchange in AE1 may not require an intracellular glutamate gate similar to channel-like ClC proteins.

S465 in the AE1 homology model corresponds to the ClC Cl^--coordinating residue, S107. AE1 transport activity is highly sensitive to S465 mutagenesis, but alanine substitutions in flanking residues of S465 had no effect on transport activity of AE1, with the exception of the G463A mutation, which may reduce helix flexibility. Mutation of ClC S107, an important chloride-coordinating residue, however, gives rise to Cl^- transport uncoupled from H^+ transport.[49] No mutagenic studies have been conducted on the residues flanking *E. coli* ClC S107. Taken together, the data suggest that AE1 S465 may be an anion coordinating site.

In the AE1 homology model, F878 corresponds to the ClC Cl^- coordinating Y445. Mutagenesis of AE1 F878 to a large alkyl or aromatic side chain had no effect on transport activity, but mutagenesis to a small alkyl or hydroxyl side chain abolished transport activity. A similar pattern of effects was observed for ClC residue Y445;[29] mutation of ClC Y445 to a large aromatic residue did not disrupt ClC transport activity, but mutation to a large alkyl residue moderately disrupted H^+-coupled Cl^- transport and mutation to small alkyl, hydroxyl, or charged residues severely disrupted H^+-coupled Cl^- transport. Thus, the data suggest that AE1 F878 has a similar role as ClC Y445 in the central Cl^- coordination site.

I791 and F792 in the AE1 homology model correspond to ClC I356 and F357, which contribute to the formation of the central Cl^- binding site through their backbone amides. I791A-AE1 had a transport activity similar to WT-AE1. F792A, which is not a conservative AE1 mutation, had a reduced transport activity. Mutations of ClC I356 and F357 might be expected to have no effect on function, but these sites have not been mutated in ClC. Together, these data are consistent with a role of I791 and F792 in Cl^- coordination through backbone groups, rather than side-chain moieties.

In our analysis of identified candidate transport mechanism residues, all mutations altered AE1 transport activity, but transport stoichiometry was unchanged on the basis of lack of changes in electrical activity. In contrast, mutation of residues critical to the ClC transport mechanism disrupted H^+-coupled Cl^- transport, thus altering the transport stoichiometry. Interestingly, variations of transport stoichiometry and substrate specificity are observed among different members of the ClC family. As discussed above, only $2Cl^-/H^+$ ClC exchangers possess an intracellular glutamate gate, which is replaced by a valine residue in Cl^- channels, such as human ClC-1 (Supplementary Fig. 4).[26] Interestingly, the $2Cl^-/H^+$ exchanger, *Cyanidioschyzon merolae* ClC (cmClC), has a threonine at the position corresponding to the intracellular glutamate gate (Supplementary Fig. 4),[27] possibly suggesting that some ion exchangers (such as AE1 and cmClC) either dispense with this gate or (as suggested[27]) have a gate located elsewhere. In addition, some plant ClC proteins function as NO_3^-/H^+ exchangers, which possess a proline residue at the position of the serine residue involved in Cl^- coordination.[50]

The AE1 homology model allowed us to identify several residues important in AE1 transport mechanism. Consistent with a role in transport mechanism, these residues (human AE1 S465, E508, and Y878) were conserved among human, mouse, and chicken AE1, as well as the two other human electroneutral Cl^-/HCO_3^- exchangers, AE2 and AE3 (Supplementary Fig. 4). Ideally, these residues could be rationalized to provide a transport mechanism for AE1. Unfortunately, the AE1 homology model provides insufficient information on the orientation of amino acid side chains. The role of the key residues identified here will be clarified upon determination of high-resolution structures of AE1 in multiple conformations.

AE1 functional studies in the context of the homology model

AE1 cysteine-scanning mutagenesis studies have been valuable in identifying AE1 pore-lining residues.[41,51] AE1 E681 was proposed to be located in a transmembrane helix near the intracellular side of the lipid bilayer. Residues on the same helical face as E681 were reactive to sulfhydryl reagents, which altered transport activity.[41] The AE1 homology model proposes that E681 forms an intracellular glutamate gate; thus, residues surrounding E681 are pore lining. Closer to the C-terminus, AE1 F806-C885 contained several pore-lining residues.[51] Interestingly, F878C-AE1 had a low transport activity compared to WT-AE1 activity of flanking mutants,[51]

which is consistent with our analysis of AE1 F878 and the surrounding region. Other residues that affect transport activity by mutagenesis or reaction with sulfhydryl reagents[51] are located in regions of the AE1 homology model that are extracellular to F878 and line the pore.

Modification of human AE1 H834 (or murine H852) with diethylpyrocarbonate or mutagenesis caused a change in anion transport activity.[52,53] Interestingly, the effects of murine H852Q-AE1 on transport activity were reversed upon mutation of K558N, which corresponds to human AE1 K539.[53] In the AE1 homology model, H834 is located close to the central Cl^- binding site, and K539 is located opposite to this histidine residue in the pore, which is consistent with the observed functional data in human and murine AE1.

Mutations in AE1 can induce a cation leak.[54–57] L687P-AE1, which has a cation leak,[55] localizes to the intracellular end of extended helix J and faces into the pore (Fig. 3). Alterations at the nearby intracellular gate, E681, could explain the induced cation leak. D705Y-AE1 also has an associated cation leak[55] and is located in the plane of the lipid bilayer, but is not a pore-forming residue in the AE1 homology model. Cation-leak-inducing S731P, R730C, and H734R-AE1[55,58] are located in the flexible region at the extracellular end of transmembrane helix L (Fig. 3). Similarly, R760Q-AE1 (Band 3 Prague II)[54] is in the extracellular loop before helix M (Fig. 3). Interestingly, cation-leak-inducing R589H, G609R, S613F, and G701D[57] are at the intracellular ends of transmembrane regions H, I, and K (Fig. 3). Location of cation-leak-forming residues, in extracellular loops and at helix ends, suggests a possible role of these regions in charge selection of substrates.

Another naturally occurring AE1 mutant, Band 3 HT (P868L), is remarkable for its increased AE1 transport activity.[59] In the AE1 homology model, this residue is located near the flexible region prior to transport mechanism residue F878, where mutations could change the structure of the central Cl^- binding site. Consistent with this possibility, we found that mutation of E508 in the central Cl^- binding site increases the transport activity of AE1.

AE1 homology model in relation to other SLC4 proteins

Analysis of other SLC4 proteins is relevant to the AE1 homology model. The AE1 transport mechanism residues, whose mutations affected transport activity, are conserved across human AE1, AE2, and AE3, suggesting a common transport mechanism across the SLC4 anion exchangers. Several histidine residues in AE2 are critical to maintain transport activity and pH sensitivity.[60] H1060A-AE2 decreases transport activity, but H1060E-AE2 has a WT level of function.[60] The homologous residue, AE1 H734, is located in the extracellular flexible region at the N-terminal end of transmembrane helix L in the AE1 homology model (Figs. 3 and 4). Close inspection of the homology model places this site at the mouth of the ion translocation pore where steric or charge effects could influence transport. Mutation of AE2 H1144 and H1145, homologous to AE1 Y818 and H819, changed extracellular pH sensitivity.[60] Interestingly, AE2 H1145 mutation also had an increased inhibition by acidic intracellular pH.[60] In the AE1 homology model, these residues are located in the extracellular loop between transmembrane helices N and O, which is consistent with extracellular pH sensing, but inconsistent with AE2 H1145 intracellular pH sensing. Murine AE2 residues involved in intracellular pH activation (R921 and R1107) and residues involved in extracellular pH activation (E888, K889, E981, K982, and D1075)[61] correspond to sites in intracellular and extracellular loops of the AE1 homology model, respectively.

NBCe1 (SLC4A4), a sodium-coupled bicarbonate transporter, and AE1 share 50% sequence similarity in their membrane domains. Cysteine-scanning mutagenesis of NBCe1 Q424–G448 suggested that this region forms part of the transmembrane ion conduction pore,[62] but the corresponding region of the AE1 homology model (Q404–G428) is not pore lining. Consistent with the AE1 homology model (F423–G428), NBCe1 F443–G448 was predicted to form an extracellular loop.[62] Interestingly, the region surrounding NBCe1 D764, corresponding to AE1 E681, is pore lining,[63] which is consistent with AE1 biochemical data and the AE1 homology model. Biochemical data from cysteine-scanning mutagenesis of NBCe1 A800-K967[64] have several differences from the corresponding study of AE1 T727–A891,[3] suggesting that NBCe1 has a C-terminal fold different from that of AE1.

Conclusion

Mutagenic analysis of AE1 presented here supports the AE1 homology model created, using *E. coli* ClC as a structural template. With the exception of the intracellular glutamate gate, transport mechanism residues predicted by the homology model were conserved. Mutation of these residues resulted in drastic changes of the AE1 transport activity. In addition, the AE1 homology model satisfies the majority of the existing biochemical constraints for the AE1 topology. The role of functionally important residues identified here will be clarified by future high-resolution AE1 structures. Until a high-resolution structure of AE1 is available, the homology model of AE1 developed here will serve as a guide for future functional and structural studies.

Materials and Methods

Materials

Oligonucleotides were from Integrated DNA Technologies (Coralville, IA). Pfx DNA polymerase, Dulbecco's modified Eagle's medium (DMEM), fetal bovine serum, calf serum, penicillin–streptomycin–glutamine, and BCECF-AM were from Invitrogen (Carlsbad, CA). T4 DNA ligase, Mung Bean nuclease, and restriction enzymes were from New England Biolabs (Ipswich, MA). QuikChange Lightning Site-Directed Mutagenesis Kit was from Agilent Technologies (Mississauga, ON, Canada). Glass coverslips were from Fisher Scientific (Ottawa, ON, Canada). BCA protein assay kit, Sulfo-NHS-SS-Biotin, and immobilized streptavidin resin were from Pierce (Rockford, IL). Nigericin and poly-L-lysine were from Sigma-Aldrich (Oakville, ON, Canada). Immobilon-P PVDF was from Millipore (Billerica, MA). ECL chemiluminescent reagent was from Perkin Elmer Life Sciences (Waltham, MA). Anti-AE1 antibody, IVF12, was a gift from Dr. Mike Jennings (University of Arkansas).[65] Donkey anti-mouse IgG conjugated to horseradish peroxidase was from GE Healthcare Bio-Sciences (Piscataway, NJ). Mouse anti-glyceraldehyde-3-phosphate dehydrogenase was from Santa Cruz Biotechnology (Santa Cruz, CA). Complete Mini-Protease Inhibitor Cocktail and collagenase A were from Roche Applied Science (Indianapolis, IN). The mMessage mMachine *in vitro* T7 RNA-polymerase kit was from Ambion (Austin, TX). Hydrogen ionophore I-cocktail A was from Fluka (Buchs, Switzerland).

Modeling

A sequence alignment of the human AE1 membrane domain (amino acids 388–911) and *E. coli* ClC was created using a published alignment,[35] with minor adjustments. This alignment was used to generate a homology model of AE1, using the *E. coli* ClC structure[26] (Protein Data Bank ID: 1OTS) as a template, with the program Modeller v9.7.[36] File containing coordinates of the AE1 model will be distributed upon request.

Molecular biology

pJRC9, which encodes WT-AE1 and vector (pRBG4), were constructed previously.[66,67] AE1 point mutants were constructed using the Agilent QuikChange Lightning Kit, primers corresponding to the mutation to be created (Supplementary Table 3), and pJRC9 as the template DNA.

pPBAE1-oocyte, which encodes WT-AE1 in an oocyte expression vector, was constructed by digesting pDEJ4,[68] with XhoI, followed by treatment with Mung Bean nuclease and HindIII. This fragment was cloned into the oocyte expression vector, pGEMHE,[69] which was digested with SmaI and HindIII, to create pPBAE1-oocyte. Oocyte expression constructs encoding S465A, E508A, M586A, D607A, I791A, and F878A-AE1 were created using the Agilent QuikChange Lightning Kit.

The oocyte expression construct for N-terminally hemagglutinin epitope (HA)-tagged glycophorin A, pSMGPA1, was created using the mammalian expression construct pHJC2 and the pGEMHE expression vector. The pHJC2 construct was created using the human glycophorin A cDNA as a PCR template, with a forward primer that encodes an N-terminal HA tag and a 5′ HindIII restriction site and a reverse primer that encodes a 3′ XhoI site. The resulting PCR product and the pcDNA3.1(–) vector were digested and ligated to create pHJC2. pHJC2 was digested with HindIII, treated with Mung Bean nuclease, further digested with XbaI, and then cloned into the SmaI/XbaI-cut oocyte expression vector pGEMHE.

Cell culture and transfection

HEK293 cells were grown at 37 °C in an air:CO_2 (19:1) environment in DMEM, supplemented with 5% (v/v) fetal bovine serum, 5% (v/v) calf serum, and 1% (v/v) penicillin–streptomycin–glutamine. cDNA encoding WT-AE1, AE1 point mutants, or vector (pRBG4) were transiently transfected in HEK293 cells by the calcium phosphate transfection method.[70] All experiments were carried out 48 h post-transfection.

Expression in *X. laevis* oocytes

Plasmid cDNA was linearized using NheI and transcribed with mMessage mMachine *in vitro* T7 RNA polymerase kit to produce capped RNA transcripts. cRNA was purified and stored at −80 °C in diethylpyrocarbonate-treated water.

X. laevis females were purchased from *Xenopus* Express, Vernassal, France. Oocytes were surgically removed under sterile conditions from anesthetized frogs and singularized by collagenase treatment in Ca^{2+}-free oocyte Ringer's solution (82.5 mM NaCl, 2.5 mM KCl, 1 mM $MgCl_2$, 1 mM Na_2HPO_4, and 5 mM Hepes, pH 7.8) at 28 °C for 1.5 h. Singularized oocytes were left to recover for approximately 16 h in HCO_3^--free oocyte Ringer's solution (Ca^{2+}-free oocyte Ringer's solution, containing 1 mM $CaCl_2$, pH 7.8). Oocytes at stage V or VI were selected and injected with 15 ng of AE1 (WT or mutant) cRNA and 1.5 ng of glycophorin A cRNA, using glass micropipettes and a microinjection device (Nanoliter 2000, World Precision Instruments, Berlin, Germany). Non-injected native oocytes were used as a control.

Immunoblotting

Samples were prepared in 2× sample buffer [10% (v/v) glycerol, 2% (w/v) SDS, 0.5% (w/v) bromophenol blue, 1% (v/v) β-mercaptoethanol, and 75 mM Tris, pH 6.8], containing Complete Mini Protease Inhibitor Cocktail. Prior to electrophoresis, samples were incubated for 4.5 min at 65 °C and insoluble material was removed by centrifugation at 16,000***g*** for 10 min. Samples were resolved on 7.5% (w/v) SDS-PAGE gels[71] and transferred to Immobilon-P PVDF membranes at 400 mA for 1 h. Membranes were subsequently blocked with TBS-TM (TBS-T [0.15 M NaCl, 50 mM Tris, and 0.1% (v/v) Tween-20, pH 7.5], containing 5% (w/v) skim milk powder) for 1 h at 20 °C. After blocking, membranes were incubated for 16 h at 4 °C in TBS-TM, containing mouse anti-AE1 antibody (IVF12)

and mouse anti-glyceraldehyde-3-phosphate dehydrogenase antibody at 1:3000 and 1:2000 dilutions, respectively. Membranes were washed three times in TBS-T, incubated with donkey anti-mouse IgG conjugated to horseradish peroxidase at a 1:5000 dilution for 1 h at 20 °C, and washed three times in TBS-T. Blots were imaged using ECL chemiluminescent reagent and visualized using a Kodak Image Station 440CF (Kodak, New York). Quantitative densitometric analysis was performed, using the Kodak Molecular Imaging Software v4.0.3 (Kodak).

Cl^-/HCO_3^- exchange assays in HEK293 cells

Anion-exchange activity of transfected HEK293 cells was monitored, using a previously described assay.[72] Briefly, HEK293 cells were grown and transfected on poly-L-lysine-treated 11 × 7.5 mm glass coverslips. Cells were rinsed in serum-free DMEM and incubated in 2 ml of serum-free DMEM, containing 2 μM BCECF-AM at 37 °C for 15 min. Coverslips were mounted in a fluorescence cuvette and perfused at 3.5 ml/min alternately with Ringer's buffer (5 mM glucose, 5 mM potassium gluconate, 1 mM calcium gluconate, 10 mM Hepes, 1 mM $MgSO_4$, 2.5 mM NaH_2PO_4, and 25 mM $NaHCO_3$, pH 7.4), containing 140 mM NaCl (chloride-containing) or 140 mM sodium gluconate (chloride-free). Both Ringer's buffers were bubbled continuously with air, containing 5% CO_2. Fluorescence was monitored using a Photon Technologies International RCR/Delta Scan spectrofluorimeter at excitation wavelengths 440 nm and 502.5 nm and emission wavelength 528.7 nm. Fluorescence measurements were converted to intracellular pH by the nigericin-high potassium method[73] with reference pH values approximately 6.5, 7.0, and 7.5. Anion-exchange activity was calculated by linear regression of the initial change (30 s) in intracellular pH upon switching from a chloride-containing to a chloride-free Ringer's buffer.

Intracellular pH and membrane current recordings in *X. laevis* oocytes

Intracellular pH and membrane potential were measured, using double-barreled microelectrodes, which have been described previously.[74] Electrodes were calibrated with bicarbonate-free oocyte Ringer's solution with a pH of 7.0 and 7.4. The recording arrangement was described previously.[74,75] Central and reference barrels of the electrodes were connected with chloride-treated silver wires to the head stages of an Axoclamp 2B amplifier (Axon Instruments, USA). In the experimental chamber, electrodes detected changes in pH faster in saline pH than the fastest reaction expected to occur in the cytoplasm of the oocyte. As described previously, optimal intracellular oocyte pH measurements were detected when the electrode was located near the intracellular surface of the plasma membrane,[76] which was achieved by carefully rotating the oocyte with the impaled electrode. Experiments were performed at 20 °C with oocytes voltage clamped at −40 mV, using two-electrode voltage clamp as described previously.[77] Oocytes were successively perfused with bicarbonate-free oocyte Ringer's solution (pH 7.4), high Cl^- oocyte Ringer's solution (57.5 mM NaCl, 2.5 mM KCl, 1 mM Na_2HPO_4, 1 mM $MgCl_2$, 1 mM $CaCl_2$, 5 mM Hepes, and 24 mM $NaHCO_3$, pH 7.4), low Cl^- oocyte Ringer's solution (57.5 mM sodium gluconate, 2.5 mM KCl, 1 mM Na_2HPO_4, 1 mM $MgCl_2$, 1 mM $CaCl_2$, 5 mM Hepes, and 24 mM $NaHCO_3$, pH 7.4), high Cl^- oocyte Ringer's solution, and bicarbonate-free oocyte Ringer's solution (pH 7.4). High and low Cl^- oocyte Ringer's solutions were bubbled continuously with 5% CO_2/95% O_2. Changes in membrane potential were monitored, during 20-mV voltage steps from −100 mV to +20 mV in each solution, to obtain current/voltage (*I*/*V*) curves.

Assays of cell surface processing

HEK293 cells were transiently transfected with cDNA encoding WT-AE1, an AE1 point mutant, or vector alone, as described above. Cells were rinsed with 4 °C phosphate-buffered saline, followed by 4 °C borate buffer (154 mM NaCl, 7.2 mM KCl, 1.8 mM $CaCl_2$, and 10 mM boric acid, pH 9.0). Cells were then incubated at 4 °C for 30 min in borate buffer, containing 0.5 mg/ml Sulfo-NHS-SS-Biotin. Cells were washed three times with quenching buffer (192 mM glycine and 25 mM Tris, pH 8.3) and solubilized for 20 min at 4 °C with 500 μl of IPB buffer (1% NP40, 5 mM ethylenediaminetetraacetic acid, 0.15 M NaCl, 0.5% deoxycholate, and 10 mM Tris, pH 7.4), containing Complete Mini Protease Inhibitor Cocktail. Cell lysates were centrifuged for 20 min at 16,000***g*** and the supernatant was collected. Half of each sample was removed for later immunoblot analysis (total protein, T). The remaining half of each sample was incubated with immobilized streptavidin resin (100 μl of a 50% slurry in phosphate-buffered saline) for 16 h at 4 °C with gentle rotation. Samples were centrifuged for 2 min at 8000***g*** and the supernatant was collected (unbound protein, U). Equal amounts of the T and U fractions were separated by SDS-PAGE and analyzed by immunoblotting as described above. Values obtained from densitometric analysis were used to calculate the percentage of protein at the cell surface with the formula (T − U)/T × 100%.

Statistical analysis

Analysis was performed using Prism software. Values are represented as the mean ± standard error. Groups were compared with one-way ANOVA and paired *t* test with $p < 0.05$ considered significant.

Acknowledgements

Pamela Bonar is supported by an Alberta Innovates Health Solutions studentship. Joseph Casey is a Scientist of Alberta Innovates Health Solutions. Support was provided by an operating grant from the Canadian Institutes of Health Research. We would like to thank Dr. Mark Glover and Dr. Joanne Lemieux for helpful advice and Dr. Arghya Basu and Sampath Loganathan for comments on the manuscript.

Supplementary Data

Supplementary data to this article can be found online at http://dx.doi.org/10.1016/j.jmb.2013.04.005

Received 21 February 2013;
Received in revised form 20 March 2013;
Accepted 3 April 2013
Available online 11 April 2013

Keywords:
Band 3;
bicarbonate transporters;
homology model;
transport mechanism;
mutagenesis

† www.psipred.com
‡ http://ekhidna.biocenter.helsinki.fi/dali_server/

Abbreviations used:
WT, wild type; BCECF-AM, 2′,7′-bis-(2-carboxyethyl)-5-(and-6)carboxylfluorescein, acetoxymethyl ester; DMEM, Dulbecco's modified Eagle's medium.

References

1. Cordat, E. & Casey, J. R. (2009). Bicarbonate transport in cell physiology and disease. *Biochem. J.* **417**, 423–439.
2. Low, P. S. (1986). Structure and function of the cytoplasmic domain of Band 3: center of erythrocyte membrane-peripheral protein interactions. *Biochim. Biophys. Acta*, **864**, 145–167.
3. Zhu, Q., Lee, D. W. & Casey, J. R. (2003). Novel topology in C-terminal region of the human plasma membrane anion exchanger, AE1. *J. Biol. Chem.* **278**, 3112–3120.
4. Grinstein, S., Ship, S. & Rothstein, A. (1978). Anion transport in relation to proteolytic dissection of Band 3 protein. *Biochim. Biophys. Acta*, **507**, 294–304.
5. Zhang, D., Kiyatkin, A., Bolin, J. T. & Low, P. S. (2000). Crystallographic structure and functional interpretation of the cytoplasmic domain of erythrocyte membrane band 3. *Blood*, **96**, 2925–2933.
6. Tang, X. B., Fujinaga, J., Kopito, R. & Casey, J. R. (1998). Topology of the region surrounding Glu681 of human AE1 protein, the erythrocyte anion exchanger. *J. Biol. Chem.* **273**, 22545–22553.
7. Fujinaga, J., Tang, X. B. & Casey, J. R. (1999). Topology of the membrane domain of human erythrocyte anion exchange protein, AE1. *J. Biol. Chem.* **274**, 6626–6633.
8. Okubo, K., Kang, D., Hamasaki, N. & Jennings, M. L. (1994). Red blood cell band 3. Lysine 539 and lysine 851 react with the same H_2DIDS (4,4'-diisothiocyano-dihydrostilbene-2,2'-disulfonic acid) molecule. *J. Biol. Chem.* **269**, 1918–1926.
9. Kang, D., Okubo, K., Hamasaki, N., Kuroda, N. & Shiraki, H. (1992). A structural study of the membrane domain of band 3 by tryptic digestion. Conformational change of band 3 in situ induced by alkali treatment. *J. Biol. Chem.* **267**, 19211–19217.
10. Jarolim, P., Rubin, H. L., Zakova, D., Storry, J. & Reid, M. E. (1998). Characterization of seven low incidence blood group antigens carried by erythrocyte band 3 protein. *Blood*, **92**, 4836–4843.
11. Pal, P., Lebedev, D., Salim, S. & Knauf, P. A. (2006). Substrates induce conformational changes in human anion exchanger 1 (hAE1) as observed by fluorescence resonance energy transfer. *Biochemistry*, **45**, 6279–6295.
12. Rao, A. & Reithmeier, R. A. F. (1979). Reactive sulfhydryl groups of the Band 3 polypeptide from human erythrocyte membranes: location in the primary structure. *J. Biol. Chem.* **254**, 6144–6150.
13. Jin, X. R., Abe, Y., Li, C. Y. & Hamasaki, N. (2003). Histidine-834 of human erythrocyte band 3 has an essential role in the conformational changes that occur during the band 3-mediated anion exchange. *Biochemistry*, **42**, 12927–12932.
14. Popov, M., Li, J. & Reithmeier, R. A. (1999). Transmembrane folding of the human erythrocyte anion exchanger (AE1, Band 3) determined by scanning and insertional N-glycosylation mutagenesis. *Biochem. J.* **339**, 269–279.
15. Bruce, L. J., Anstee, D. J., Spring, F. A. & Tanner, M. J. (1994). Band 3 Memphis variant II. Altered stilbene disulfonate binding and the Diego (Dia) blood group antigen are associated with the human erythrocyte band 3 mutation Pro854→Leu. *J. Biol. Chem.* **269**, 16155–16158.
16. Casey, J. R. & Reithmeier, R. A. F. (1991). Analysis of the oligomeric state of Band 3, the anion transport protein of the human erythrocyte membrane, by size exclusion high performance liquid chromatography: oligomeric stability and origin of heterogeneity. *J. Biol. Chem.* **266**, 15726–15737.
17. Taylor, A. M., Zhu, Q. & Casey, J. R. (2001). Cysteine-directed cross-linking localizes regions of the human erythrocyte anion exchange protein (AE1) relative to the dimeric interface. *Biochem. J.* **359**, 661–668.
18. Groves, J. D. & Tanner, M. J. (1999). Structural model for the organization of the transmembrane spans of the human red-cell anion exchanger (band 3; AE1). *Biochem. J.* **344**, 699–711.
19. Yamaguchi, T., Ikeda, Y., Abe, Y., Kuma, H., Kang, D., Hamasaki, N. & Hirai, T. (2010). Structure of the membrane domain of human erythrocyte anion exchanger 1 revealed by electron crystallography. *J. Mol. Biol.* **397**, 179–189.
20. Joanne Lemieux, M., Reithmeier, R. A. & Wang, D. N. (2002). Importance of detergent and phospholipid in the crystallization of the human erythrocyte anion-exchanger membrane domain. *J. Struct. Biol.* **137**, 322–332.
21. Wang, D. N., Sarabia, V. E., Reithmeier, R. A. & Kuhlbrandt, W. (1994). Three-dimensional map of

the dimeric membrane domain of the human erythrocyte anion exchanger, Band 3. *EMBO J.* **13**, 3230–3235.
22. Wang, D. N., Kuhlbrandt, W., Sarabia, V. & Reithmeier, R. A. F. (1993). Two-dimensional structure of the membrane domain of human band 3, the anion transport protein of the erythrocyte membrane. *EMBO J.* **12**, 2233–2239.
23. Jiang, J., Magilnick, N., Tsirulnikov, K., Abuladze, N., Atanasov, I., Ge, P. *et al.* (2013). Single particle electron microscopy analysis of the bovine anion exchanger 1 reveals a flexible linker connecting the cytoplasmic and membrane domains. *PLoS One*, **8**, e55408.
24. Casey, J. R., Lieberman, D. M. & Reithmeier, R. A. F. (1989). Purification and characterization of Band 3 protein. *Methods Enzymol.* **173**, 494–512.
25. Jentsch, T. J., Stein, V., Weinreich, F. & Zdebik, A. A. (2002). Molecular structure and physiological function of chloride channels. *Physiol. Rev.* **82**, 503–568.
26. Dutzler, R., Campbell, E. B., Cadene, M., Chait, B. T. & MacKinnon, R. (2002). X-ray structure of a ClC chloride channel at 3.0 Å reveals the molecular basis of anion selectivity. *Nature*, **415**, 287–294.
27. Feng, L., Campbell, E. B., Hsiung, Y. & MacKinnon, R. (2010). Structure of a eukaryotic CLC transporter defines an intermediate state in the transport cycle. *Science*, **330**, 635–641.
28. Dutzler, R., Campbell, E. B. & MacKinnon, R. (2003). Gating the selectivity filter in ClC chloride channels. *Science*, **300**, 108–112.
29. Walden, M., Accardi, A., Wu, F., Xu, C., Williams, C. & Miller, C. (2007). Uncoupling and turnover in a Cl^-/H^+ exchange transporter. *J. Gen. Physiol.* **129**, 317–329.
30. Robertson, J. L., Kolmakova-Partensky, L. & Miller, C. (2010). Design, function and structure of a monomeric ClC transporter. *Nature*, **468**, 844–847.
31. Jennings, M. L. & Passow, H. (1979). Anion transport across the erythrocyte membrane *in situ* proteoysis of Band 3 protein, and cross-linking of proteolytic fragments by 4,4'-diisothiocyano dihydrostilbene-2,2'-disulfonate. *Biochim. Biophys. Acta*, **554**, 498–519.
32. Accardi, A. & Picollo, A. (2010). CLC channels and transporters: proteins with borderline personalities. *Biochim. Biophys. Acta*, **1798**, 1457–1464.
33. Jennings, M. L. (1989). Structure and function of the red blood cell anion transport protein. *Annu. Rev. Biophys. Biophys. Chem.* **18**, 397–430.
34. Ohana, E., Shcheynikov, N., Yang, D., So, I. & Muallem, S. (2011). Determinants of coupled transport and uncoupled current by the electrogenic SLC26 transporters. *J. Gen. Physiol.* **137**, 239–251.
35. Hirai, T., Hamasaki, N., Yamaguchi, T. & Ikeda, Y. (2011). Topology models of anion exchanger 1 that incorporate the anti-parallel V-shaped motifs found in the EM structure. *Biochem. Cell Biol.* **89**, 148–156.
36. Sali, A. & Blundell, T. L. (1993). Comparative protein modelling by satisfaction of spatial restraints. *J. Mol. Biol.* **234**, 779–815.
37. Kopito, R. R. & Lodish, H. F. (1985). Primary structure and transmembrane orientation of the murine anion exchange protein. *Nature*, **316**, 234–238.
38. Chernova, M. N., Jiang, L., Crest, M., Hand, M., Vandorpe, D. H., Strange, K. & Alper, S. L. (1997). Electrogenic sulfate/chloride exchange in *Xenopus* oocytes mediated by murine AE1 E699Q. *J. Gen. Physiol.* **109**, 345–360.
39. Jennings, M. L. (2005). Evidence for a second binding/transport site for chloride in erythrocyte anion transporter AE1 modified at glutamate 681. *Biophys. J.* **88**, 2681–2691.
40. Jennings, M. L. & Smith, J. S. (1992). Anion–proton cotransport through the human red blood cell band 3 protein. Role of glutamate 681. *J. Biol. Chem.* **267**, 13964–13971.
41. Tang, X.-B., Kovacs, M., Sterling, D. & Casey, J. R. (1999). Identification of residues lining the translocation pore of human AE1, plasma membrane anion exchange protein. *J. Biol. Chem.* **274**, 3557–3564.
42. Groves, J. D. & Tanner, M. J. (1992). Glycophorin A facilitates the expression of human Band 3-mediated anion transport in *Xenopus* oocytes. *J. Biol. Chem.* **267**, 22163–22170.
43. Abramson, J., Smirnova, I., Kasho, V., Verner, G., Kaback, H. R. & Iwata, S. (2003). Structure and mechanism of the lactose permease of *Escherichia coli*. *Science*, **301**, 610–615.
44. Smirnova, I., Kasho, V., Choe, J. Y., Altenbach, C., Hubbell, W. L. & Kaback, H. R. (2007). Sugar binding induces an outward facing conformation of LacY. *Proc. Natl Acad. Sci. USA*, **104**, 16504–16509.
45. Bartel, D., Hans, H. & Passow, H. (1989). Identification by site-directed mutagenesis of lys-558 as the covalent attachment site of H_2DIDS in the mouse erythroid Band 3 protein. *Biochim. Biophys. Acta*, **985**, 355–358.
46. Vince, J. W. & Reithmeier, R. A. (2000). Identification of the carbonic anhydrase II binding site in the Cl^-/HCO_3^- anion exchanger AE1. *Biochemistry*, **39**, 5527–5533.
47. Accardi, A. & Miller, C. (2004). Secondary active transport mediated by a prokaryotic homologue of ClC Cl^- channels. *Nature*, **427**, 803–807.
48. Lim, H. H. & Miller, C. (2009). Intracellular proton-transfer mutants in a CLC Cl^-/H^+ exchanger. *J. Gen. Physiol.* **133**, 131–138.
49. Jayaram, H., Accardi, A., Wu, F., Williams, C. & Miller, C. (2008). Ion permeation through a Cl-selective channel designed from a CLC Cl^-/H^+ exchanger. *Proc. Natl Acad. Sci. USA*, **105**, 11194–11199.
50. De Angeli, A., Monachello, D., Ephritikhine, G., Frachisse, J. M., Thomine, S., Gambale, F. & Barbier-Brygoo, H. (2006). The nitrate/proton antiporter AtCLCa mediates nitrate accumulation in plant vacuoles. *Nature*, **442**, 939–942.
51. Zhu, Q. & Casey, J. R. (2004). The substrate anion selectivity filter in the human erythrocyte Cl^-/HCO_3^- exchange protein, AE1. *J. Biol. Chem.* **279**, 23565–23573.
52. Takazaki, S., Abe, Y., Yamaguchi, T., Yagi, M., Ueda, T., Kang, D. & Hamasaki, N. (2010). Mutation of His 834 in human anion exchanger 1 affects substrate binding. *Biochim. Biophys. Acta*, **1798**, 903–908.
53. Müller-Berger, S., Karbach, D., Konig, J., Lepke, S., Wood, P. G., Appelhans, H. & Passow, H. (1995). Inhibition of mouse erythroid band 3-mediated chloride transport by site-directed mutagenesis of histidine residues and its reversal by second site mutation of

Lys 558, the locus of covalent H_2DIDS binding. *Biochemistry*, **34**, 9315–9324.
54. Bruce, L. J., Robinson, H. C., Guizouarn, H., Borgese, F., Harrison, P., King, M. J. *et al.* (2005). Monovalent cation leaks in human red cells caused by single amino-acid substitutions in the transport domain of the band 3 chloride-bicarbonate exchanger, AE1. *Nat. Genet.* **37**, 1258–1263.
55. Guizouarn, H., Martial, S., Gabillat, N. & Borgese, F. (2007). Point mutations involved in red cell stomatocytosis convert the electroneutral anion exchanger 1 to a non-selective cation conductance. *Blood*, **110**, 2158–2165.
56. Ellory, J. C., Guizouarn, H., Borgese, F., Bruce, L. J., Wilkins, R. J. & Stewart, G. W. (2009). Review. Leaky $Cl–HCO_3^-$ exchangers: cation fluxes via modified AE1. *Philos. Trans. R. Soc. Lond. B Biol. Sci.* **364**, 189–194.
57. Walsh, S., Borgese, F., Gabillat, N., Unwin, R. & Guizouarn, H. (2008). Cation transport activity of anion exchanger 1 mutations found in inherited distal renal tubular acidosis. *Am. J. Physiol. Renal Physiol.* **295**, F343–F350.
58. Stewart, A. K., Kedar, P. S., Shmukler, B. E., Vandorpe, D. H., Hsu, A., Glader, B. *et al.* (2011). Functional characterization and modified rescue of novel AE1 mutation R730C associated with overhydrated cation leak stomatocytosis. *Am. J. Physiol. Cell Physiol.* **300**, C1034–C1046.
59. Bruce, L. J., Kay, M. M. B., Lawrence, C. & Tanner, M. J. A. (1993). Band 3 HT, a human red cell variant associated with acanthocytosis and increased anion transport, carries the mutation Pro-868 ∅ Leu in the membrane domain of band 3. *Biochem. J.* **293**, 317–320.
60. Stewart, A. K., Kurschat, C. E., Burns, D., Banger, N., Vaughan-Jones, R. D. & Alper, S. L. (2007). Transmembrane domain histidines contribute to regulation of AE2-mediated anion exchange by pH. *Am. J. Physiol. Cell Physiol.* **292**, C909–C918.
61. Stewart, A. K., Kurschat, C. E. & Alper, S. L. (2007). Role of nonconserved charged residues of the AE2 transmembrane domain in regulation of anion exchange by pH. *Pflugers Arch.* **454**, 373–384.
62. Zhu, Q., Azimov, R., Kao, L., Newman, D., Liu, W., Abuladze, N. *et al.* (2009). NBCe1-A transmembrane segment 1 lines the ion translocation pathway. *J. Biol. Chem.* **284**, 8918–8929.
63. McAlear, S. D. & Bevensee, M. O. (2006). A cysteine-scanning mutagenesis study of transmembrane domain 8 of the electrogenic sodium/bicarbonate cotransporter NBCe1. *J. Biol. Chem.* **281**, 32417–32427.
64. Zhu, Q., Kao, L., Azimov, R., Abuladze, N., Newman, D., Pushkin, A. *et al.* (2010). Structural and functional characterization of the C-terminal transmembrane region of NBCe1-A. *J. Biol. Chem.* **285**, 37178–37187.
65. Jennings, M. L., Anderson, M. P. & Monaghan, R. (1986). Monoclonal antibodies against human erythrocyte Band 3 protein: localization of proteolytic cleavage sites and stilbenedisulfonate-binding lysine residues. *J. Biol. Chem.* **261**, 9002–9010.
66. Casey, J. R., Ding, Y. & Kopito, R. R. (1995). The role of cysteine residues in the erythrocyte plasma membrane anion exchange protein, AE1. *J. Biol. Chem.* **270**, 8521–8527.
67. Lee, B. S., Gunn, R. B. & Kopito, R. R. (1991). Functional differences among nonerythroid anion exchangers expressed in a transfected human cell line. *J. Biol. Chem.* **266**, 11448–11454.
68. Johnson, D. E. & Casey, J. R. (2011). Cytosolic H^+ microdomain developed around AE1 during AE1-mediated Cl^-/HCO_3^- exchange. *J. Physiol.* **589**, 1551–1569.
69. Liman, E. R., Tytgat, J. & Hess, P. (1992). Subunit stoichiometry of a mammalian K^+ channel determined by construction of multimeric cDNAs. *Neuron*, **9**, 861–871.
70. Ruetz, S., Lindsey, A. E. & Kopito, R. R. (1993). Function and biosynthesis of erythroid and nonerythroid anion exchangers. *Soc. Gen. Physiol. Ser.* **48**, 193–200.
71. Laemmli, U. K. (1970). Cleavage of structural proteins during assembly of the head of bacteriophage T4. *Nature*, **227**, 680–685.
72. Loiselle, F. B. & Casey, J. R. (2003). Measurement of Cell pH. *Methods Mol. Biol.* **227**, 259–280.
73. Thomas, J. A., Buchsbaum, R. N., Zimniak, A. & Racker, E. (1979). Intracellular pH measurements in Ehrlich ascites tumor cells utilizing spectroscopic probes generated in situ. *Biochemistry*, **18**, 2210–2218.
74. Deitmer, J. W. (1991). Electrogenic sodium-dependent bicarbonate secretion by glial cells of the leech central nervous system. *J. Gen. Physiol.* **98**, 637–655.
75. Munsch, T. & Deitmer, J. W. (1994). Sodium-bicarbonate cotransport current in identified leech glial cells. *J. Physiol.* **474**, 43–53.
76. Broer, S., Schneider, H. P., Broer, A., Rahman, B., Hamprecht, B. & Deitmer, J. W. (1998). Characterization of the monocarboxylate transporter 1 expressed in *Xenopus laevis* oocytes by changes in cytosolic pH. *Biochem. J.* **333**, 167–174.
77. Becker, H. M. & Deitmer, J. W. (2007). Carbonic anhydrase II increases the activity of the human electrogenic Na^+/HCO_3^- cotransporter. *J. Biol. Chem.* **282**, 13508–13521.